Journal of
Ceramic Science
and Technology

J. Ceram. Sci. Tech., 07 [02] 209-222 (2016)
DOI: 10.4416/JCST2016-00024
available online at: http://www.ceramic-science.com

Carbon-Bonded Alumina Refractories with Reduced Carbon Content due to the Addition of Semi-Conductive Silicon and/or Nanoparticles

N. Brachhold*[1], J. Fruhstorfer[1], A. Mertke[2], C.G. Aneziris[1]

[1]TU Bergakademie Freiberg, Institute of Ceramic,
Glass and Construction Materials, Agricolastr. 17, D-09599 Freiberg
[2]Salzgitter Mannesmann Forschung GmbH, Eisenhüttenstrasse 99, D-38239 Salzgitter
received March 15, 2016; received in revised form May 1, 2016; accepted May 3, 2016

Abstract

This study investigated the combined effect of nanoscaled additives (carbon nanotubes and nanoscaled alumina) and semi-conductive silicon on carbon-bonded alumina with a reduced primary carbon content of 20 wt%. It focused on the initial cold modulus of rupture and its evolution on exposure to thermal shock. The use of the single additive groups or their combination yielded an increased initial strength compared to the reference without additives. It was shown that the combination of the additives resulted in a material that exhibited no statistically significant decrease of the cold modulus of rupture in up to five thermal shock cycles. To understand these effects, physical properties (total porosity, open porosity, true density) were observed. The data showed that the microstructural reactions were complex. The combination of all additives caused a decrease in the open porosity. The available data of the true density analysis matched partly with the possible reactions. Especially the formation of SiC whiskers was considered to be important during the coking process and the thermal shocks. Furthermore, it was proposed that a deposition of carbon because of oxidation processes followed by reactions with the additives, especially the semi-conductive silicon, occurred, which might have a self-healing effect on the refractory matrix.

Keywords: Nanoscaled additives, silicon, carbon-bonded alumina, semi-conductive material, reduced graphite

I. Introduction

In the steelmaking process, numerous functional components such as submerged entry nozzles, monobloc stoppers and ladle shrouds are made of carbon-bonded alumina (Al_2O_3-C) on account of its high performance in terms of mechanical strength, thermal shock resistance and corrosion resistance [1].

These excellent properties result from the components of the Al_2O_3-C-system, namely alumina, graphite and an organic binder as bonding medium and carbon source. Alumina is well known for its high corrosion, erosion and abrasion resistance in refractory applications. Graphite exhibits very high refractoriness owing to its sublimation point at approximately 4000 K [2] and a very low wettability on exposure to molten metals and slags [1,3]. Furthermore, it provides excellent thermal shock resistance because of its low coefficient of thermal expansion ($\approx 10\ldots50\cdot10^{-7}$ K^{-1}) and its high thermal conductivity (≈ 80 $Wm^{-1}K^{-1}$). The combination of alumina and graphite leads to a composite refractory material with improved slagging resistance and thermal shock performance. The thermal shock performance is an essential property for functional components like submerged entry nozzles because these have to withstand the beginning of the casting process during continuous steel casting. In this case, the functional components are preheated up to 1100 °C and an interval of approximately 500 K has to be bridged when the hot metal melt contacts the carbon-bonded alumina component. The composite material based on Al_2O_3-C exhibits lower thermal expansion, a lower Young's modulus of elasticity, higher thermal conductivity and higher elongation than pure Al_2O_3 [4].

The organic binder as the third component in carbon-bonded refractories is commonly based on phenolic resins. They are condensation products of phenol and formaldehyde [5]. According to the catalytic environment, two types of phenolic resins are distinguished, namely resol (alkaline catalytically driven process) and novolac (acidic catalytically driven process). The polymerization process is based on the reaction of hydroxymethyl groups (-CH_2OH) in the system. Resol binder systems contain these groups. Novolac systems need additionally hexamethylenetetramine (Hexa) to provide hydroxymethyl groups. The polymerization process (also curing or hardening process) takes place at temperatures above 160 °C with the splitting off of water molecules (resol) or ammonia (novolac) [5]. The reaction results in a three-dimensional cross-linked lattice (resite lattice), which is very hard, insoluble and not meltable. At ambient temperature and standard pressure, phenolic resins are solid substances. The pulverized solid phenolic resin can either be directly used as binder or the resin is introduced into the system as liquid resin after the solid material has been dissolved in an organic solvent.

* Corresponding author: nora.brachhold@ikgb.tu-freiberg.de

During a coking process at elevated temperatures (approx. 700 °C or more), the resite lattice transforms into essentially elementary carbon to form the bonding matrix between alumina and primarily added carbon raw materials such as graphite. Theoretically a binder carbon yield of about 75 wt% is possible, which describes the ratio of the residual carbon weight to the initial binder weight [5]. Typically, values of 40 – 55 wt% are achieved under practical conditions. The resulting carbon lattice is the so-called glassy carbon lattice because it consists of belt-like graphitic areas without regular crystalline order and many vacancies. Owing to this structure, glassy carbon has a lower density and isotropic properties in terms of electrical and thermal conductivities in comparison to graphite. However, it is highly susceptible to oxidation and attack by oxidizing melts owing to its large inner surface [2,6,7].

The resulting composite material Al_2O_3-C contains approximately 30 wt% carbon and 70 wt% alumina. On the one hand, the carbon content results from the primarily added carbon raw materials (primary carbon), which consists mainly of elementary carbon, such as graphite. On the other hand, the carbon content results from the carbon fraction in the organic binder system, which transforms to carbon in carbonization processes during the coking process (secondary carbon). Al_2O_3-C is a common heavy-duty material used in the steelmaking process. However, it has to contend with numerous challenges in steel production technology today. Firstly, increasingly cost-effective production with higher throughput is required, meaning that a longer service life of the refractories is necessary. To meet this requirement, research on innovative refractories with improved properties is important. Secondly, the issue of environmental protection is increasingly relevant in all industrial processes [8,9]. Carbon-bonded refractories cause harmful emissions – mainly during the manufacturing process and partly during their service life owing to the carbon-based components in the system. Therefore, a reduction of the carbon content in the refractories has to be sought to reduce these environmentally relevant emissions. Thirdly, the sector of ultra-low carbon steels is becoming increasingly important. These steel types tend to incorporate carbon into their structure when in contact with carbon-bonded refractories. This carbon pick-up causes a downgrading of the steel properties. A further advantage of lower carbon content in Al_2O_3-C systems are the lower thermal losses owing to its lower thermal conductivity as long as the thermal shock performance of the material is sufficient. Al_2O_3-C- materials with higher thermal insulation properties can lead to improved control of the temperature profile in casting processes and secure the high quality of steel thanks to improved flow control. The optimization of the thermal conductivity is especially important from the economic and environmental point of view. The loss of thermal energy causing a temperature decrease of 1 K results in additional costs of approximately 0.05 € per tonne steel [10]. So, these issues show that ongoing optimization of Al_2O_3-C is necessary because the reduction of the carbon content strongly affects the properties of the refractory system.

These challenges can be met by tailoring the microstructure of the bonding matrix. A first approach to influence the microstructure to improve its oxidation resistance, which corresponds to an increased service lifetime, is the use of antioxidants [11–18]. Typical antioxidants are metallic powders (e.g. Al or Si with a particle size up to 150 µm) and carbides or boron-containing oxides (with a particle size up to 100 µm). The antioxidative mechanism is based on oxidative reactions forming CO(g) (from the carbon matrix) and forming gaseous metal oxides (from the antioxidants) [12]. Both gaseous species react together, resulting in the reduction of CO(g) by the gaseous metal oxides to form solid C again. This reduces the carbon loss in the presence of oxygen. Such reactions can be accompanied by the formation of oxidic sealing layers, which protect the refractory from further oxidation processes, or by volume expansions reducing porosity [16]. Furthermore, the formation of whiskers or plate-like structures is possible, which improves the mechanical properties of the materials [12].

A second approach is the use of nanoscaled materials such as carbon nanotubes or nanoscaled oxides (e.g. alumina, magnesium aluminate spinel). These are supposed to yield a better connection between the coarse grains and the carbon matrix based on the formation of new bonding phases like Al_3CON as proposed by Roungos *et al.* [4,19]. In that study, the resulting improvement of the cold modulus of rupture and the thermal shock performance permitted a reduction in the primary carbon content from 30 wt% to 20 wt%.

Thirdly, the use of n-type semi-conductive additives able to emit electrons at elevated temperatures is proposed. It has been proposed that such additives increase the binder carbon yield based on the transfer of electrons during the coking process and during the following thermal load [20–25].

In the present study, the combined effect of nanoscaled additives (carbon nanotubes and nanoscaled Al_2O_3) and of semi-conductive silicon (P-doped) in metallic-silicon-containing carbon-bonded alumina was investigated. The metallic silicon, working as an antioxidant, was partly replaced with semi-conductive silicon. The aim was to investigate if the combination of these additives yielded a further improvement of the cold modulus of rupture and the thermal shock performance of Al_2O_3-C [4,19,24,25]. The study concentrated on Al_2O_3-C with additives and 20 wt% graphite as primary carbon, which corresponds to an already reduced content of primary carbon in comparison with conventional material containing 30 wt% primary carbon.

II. Experimental

The alumina component of the samples in this study consisted of two different alumina fractions. White fused alumina (99.46 wt% Al_2O_3, 0.45 wt% Na_2O, d_{50} = 76.40 µm) with a maximum grain size of 0.2 mm (Treibacher Industrie AG, Althofen, Austria) was used as the fine fraction. Tabular alumina (99.50 wt% Al_2O_3, max. 0.4 wt% Na_2O, d_{50} = 0.35 mm) with a maximum grain size of 0.60 mm (Almatis GmbH, Ludwigshafen, Germany) constituted the coarse fraction. Graphite was introduced into the samples in the form of two graphite sources. On the one hand,

Table 1: Additives (nano-scaled particles and semi-conductive silicon).

Additives	Producer	Abbreviation	Purity	Average particle size			Specific surface area	Specific resistance	Doping
			wt.-%				m^2/g	(Ohm cm)	
Carbon Nanotubes (C)	Timesnano (China)	TN	≥95.00	Outer Diameter >50 nm	Inner Diameter 5 – 15 nm	Length 10 – 20 µm	>40.00	-	-
Alumina nanosheets (α-Al_2O_3)	Sawyer (USA)	AS	95.00 – 99.80	10 – 250 nm			9 – 40	-	-
Silicon	Silchem, (Germany)	Si (special)	-	< 64 µm			-	1.20 – 1.30	Phosphorous

natural graphite with a very fine grain size distribution (99.50 wt% < 40 µm, d_{50} = 8.50 – 11.00 µm) and with a carbon content of 90 – 96 wt% was used as raw material, and on the other hand, flaked, coarse-grade graphite (95.00 wt% > 71 µm, d_{50} = 140 µm) with 87 – 98 wt% carbon content. Both graphite types were produced by Graphit Kropfmühl AG, Hauzenberg, Germany. The metallic silicon powder added as a high-purity antioxidant (99.50 wt% < 150 µm, d_{50} = 17.30 µm) was supplied by Elkem, Oslo, Norway. In addition to these raw materials, different nanoscaled materials and a semi-conductive silicon as listed in Table 1 were used. In all experiments, a liquid (PF 7280 FL 01) and a powder phenolic resin (0235 DP), both from Momentive Specialty Chemicals, Iserlohn, Germany, were added as binders. Furthermore, hexamethylenetetramine (Momentive Specialty Chemicals, Iserlohn, Germany) was used as a curing agent. In Table 2, the investigated compositions with 20 wt% primary carbon are listed.

The same production method was used for all Al_2O_3-C samples and is comparable to standard industrial practice and close to the mixing range described by Kunz [26]. Firstly, the two alumina grains where mixed together for 1 min in an Eirich compulsory mixer RV02 (Maschinenfabrik Gustav Eirich GmbH & Co KG, Hardheim, Germany) at room temperature. Afterwards, the liquid resin was added and mixed with the alumina grains for 3 min. Right after the liquid resin, the additives (nanoparticle and/or semi-conductive silicon) were added. This mixing order ensured homogeneous distribution of the additives and prevented leak-out of the nanoparticles. In a further step, the silicon was added and mixed for 3 min followed by the two grades of graphite, which were also mixed for 3 min. Finally, the solid resin and the curing agent were added. After further mixing for 5 min, the mixtures were uniaxially pressed to bars (25 x 25 x150 mm^3) at 100 MPa using a uniaxial press (RUCKS Maschinenbau GmbH, Glauchau, Germany).

The pressed samples were cured in a dryer (Model TR 120 from Nabertherm GmbH, Lilienthal, Germany). They were heated in steps (in 20 min up to 85 °C with a dwell time of 90 min, in 30 min up to 120 °C with a dwell time of 120 min, in 150 min up to 180 °C) up to 180 °C, and held at that temperature for 90 min. Afterwards, all samples were coked for 5 h at a temperature of 1000 °C in reducing atmosphere in an electric chamber furnace (Model LH 15/14, Nabertherm GmbH, Lilienthal, Germany). To provide a reducing atmosphere, the samples were placed in a retort filled with petrol coke during the coking process. The coking temperature was chosen according to the investigations by Roungos *et al.* [4] and Stein *et al.* [24]. The heating rate was 3 K/min.

Table 2: Compositions of the investigated samples.

Raw materials	Compositions (wt%)			
	Reference R20	R20-SiTNAS	R20-Si	R20-TNAS
Fused alumina	29.10	29.10	29.10	29.10
Tabular alumina	38.90	38.90	38.90	38.90
Fine graphite	10.00	10.00	10.00	10.00
Coarse graphite	10.00	10.00	10.00	10.00
Novolac liquid	2.00	2.00	2.00	2.00
Novolac powder	4.00	4.00	4.00	4.00
Metallic silicon	6.00	5.50	5.50	6.00
Hexa.	0.60	0.60	0.60	0.60
Carbon nanotubes		0.30		0.30
Alumina nanosheets		0.10		0.10
Si (special)		0.50	0.50	

The microstructure was examined with the aid of an environmental scanning electron microscope (ESEM, Philips Type XL30). Additionally, the bulk density and the extent of the open porosity of the coked samples were measured according to DIN EN 993 – 1 with toluene as the intrusion liquid. The true density was measured with He-pycnometry (AccuPyc 1330, Micromeritics, Aachen, Germany)

Table 3: Cold modulus of rupture (CMOR) and thermal shock behavior.

Composition	CMOR [MPa]	$CMOR_{1TS}$ [MPA]	$CMOR_{5TS}$ [MPa]	$\Delta TS_{(0\rightarrow1)}$ [%]	$\Delta TS_{(1\rightarrow5)}$ [%]
R20	10.31±0.15	6.95±0.36	6.65±0.45	-32,58	-4,41
R20-Si	13.20±1.13	9.66±1.53	8.01±0.38	-26,77	-17,14
R20-TNAS	12.56±1.40	11.92±1.41	9.38±0.75	-5,07	-21,33
R20-SiTNAS	14.51±0.26	12.11±0.81	13.89±0.96	-16,54	14,64

according to DIN 66137 – 2. Furthermore, the mechanical properties of the samples were determined by measuring their cold modulus of rupture (CMOR) according to DIN EN 993 – 6 (TIRA Test 28100, TIRA GmbH, Schalkau, Germany). The thermal shock resistance of the investigated materials was determined. The samples were quenched from 950 °C with compressed air in accordance with DIN EN 993 – 11. Afterwards, the retained CMOR was measured after one and five thermal shock cycles for all material types in line with Fruhstorfer *et al.* [27]. Finally, the carbon content of the samples after coking was measured with an elementary analyser vario MICRO cube (Elementar Analysensysteme GmbH, Hanau, Germany). The residual carbon binder yield was calculated according to Stein [22].

III. Results and Discussion

The cold modulus of rupture (CMOR) was investigated to observe phenomenologically the possible combined effect of the nanoscaled additives (TN and AS) and semi-conductive silicon. The CMOR was then related to the physical properties open porosity, total porosity, true density and binder carbon yield to facilitate understanding of the differences between the material systems and their effects on CMOR evolution. Additionally, SEM images of the microstructure were taken into account.

(1) Evolution of the cold modulus of rupture

To investigate the combined effect of nanoscaled additives and semi-conductive silicon on carbon-bonded alumina, this study concentrated in the first place on the evolution of the cold modulus of rupture (CMOR) of the investigated samples. Fig. 1 and Table 3 show the test results for the material after coking and for samples after one and five thermal shock cycles (TS). They include the relative strength change after the first thermal shock cycle compared to the initial state ($\Delta TS_{0\rightarrow1}$) and after the fifth thermal shock cycle compared to the first one ($\Delta TS_{1\rightarrow5}$). Table 5 presents an analysis of variance (ANOVA) to evaluate the effect of the factors 'additive combination' (AC) and 'number of thermal shock cycles' (TS) on the CMOR.

An ANOVA [28] applies the t-test to more than two variables or factors and tests the means of the observations corresponding to the investigated variables on their difference. The null hypothesis is that all means are equal. For each observation, a probability is calculated, the so-called *p*-value, which corresponds to the probability that the mean in question will take a value as the observed value. The lower this probability is, the higher is the evidence against the null hypothesis. Usually, the effect of a factor is considered to be significant if its *p*-value is < 0.05.

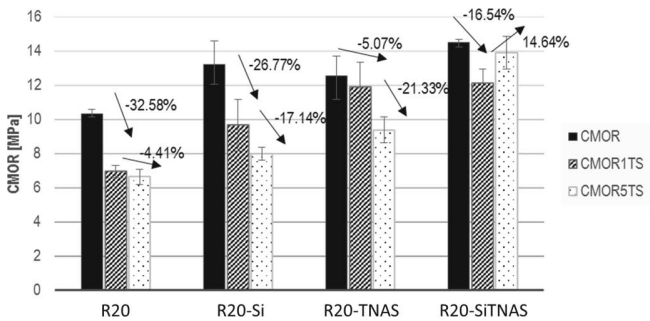

Fig. 1: CMOR of the samples after coking (CMOR), after one thermal shock (CMOR1TS) and after five thermal shocks (CMOR5TS).

Table 4 shows that both investigated factors had a significant effect on the CMOR. Additionally, the interaction between AC and TS had a significant influence, which indicated that the factors did not independently control the CMOR. Table 5 presents the means of the CMOR for the different levels of the investigated factors to determine the direction of their influence. Additionally, Tukey tests were performed. Based on pairwise comparisons, they permit identification of significant differences in the main effects or the interactions of two groups of samples.

Table 4: *p*-values of the analysis of variance for the cold modulus of rupture (CMOR) (significant effects on a level ≤ 0.05 marked in italic and on a level ≤ 0.001 bold).

Factor[a]	*p*-value
AC	$6.1 \cdot 10^{-11}$
TS	$2.9 \cdot 10^{-8}$
AC:TS	0.0015

[a] AC – Additive Combination, TS – Number of thermal shock cycles, AC:TS – Interactions

Table 5: Table of means of the significant factors for the cold modulus of rupture (CMOR).

Significant factor[a]		CMOR [MPa]			
AC		R20	R20-Si	R20-TNAS	R20-SiTNAS
		7.97	10.29	11.29	13.50
TS		0	1	5	
		12.65	10.16	9.48	
AC:TS	AC:	R20	R20-Si	R20-TNAS	R20-SiTNAS
	TS: 0	10.31	13.20	12.56	14.51
	1	6.95	9.66	11.92	12.11
	5	6.65	8.00	9.38	13.89

[a] AC – Additive Combination, TS – Number of thermal shock cycles, AC:TS - Interactions

The factor 'additive combination' (AC) increased the CMOR according to the sequence no additive (R20) → semi-conductive Si (R20-Si) → nanoscaled TN&AS (R20-TNAS) → complete additive combination (R20-SiTNAS). The pairwise comparisons in the Tukey test are summarized in Table 6. It shows that there was a significant difference in the behavior of all groups except the pair R20-TNAS – R20-Si. This means that the use of one additive (semi-conductive Si – R20-Si – or nanoscaled additives TN&AS – R20-TNAS) increased the CMOR significantly in comparison to the R20 samples, which contained no additive. This confirmed the results of Roungos *et al.*[4] and Stein *et al.*[24], who performed first investigations with the same single additive varieties in the system Al_2O_3-C. The combined application of semi-conductive Si and TN&AS in the sample group R20-SiTNAS resulted in a significant further increase of the CMOR level compared to the reference R20 and the other groups using the single additives (semi-conductive Si – R20-Si – or nanoscaled additives TN&AS – R20-TNAS).

Table 6: Tukey-test for the pairwise comparison of the cold modulus of rupture (CMOR) (x – values significantly different, – values not significantly different).

	R20-Si	R20-TNAS	R20-SiTNAS
R20	x	x	x
R20-SiTNAS	x	x	
R20-TNAS	-		

The factor 'number of thermal shock cycles' (TS) decreased the CMOR with increasing thermal shock number. The pairwise comparison between the sample groups of the same thermal shock numbers showed that the CMOR changes $\Delta TS_{0\rightarrow1}$ and $\Delta TS_{1\rightarrow5}$ were significant.

The analysis of the interaction AC:TS using the pairwise comparison of the Tukey test revealed some additional features in the evolution of the CMOR. It showed that in the coked state the initial $CMOR_{0TS}$ improved in the samples R20-Si and R20-SiTNAS in comparison with the reference R20. The $CMOR_{0TS}$ of these two sample groups R20-Si and R20-SiTNAS did not differ significantly. In contrast to this observation, the addition of TN&AS (R20-TNAS) did not yield a significant increase of the $CMOR_{0TS}$ in the coked state in comparison to the reference R20.

Under thermal shock load, the sample groups behaved very differently, too. For the samples R20 and R20-Si, the first CMOR change $\Delta TS_{0\rightarrow1}$ was significant. By contrast, $\Delta TS_{1\rightarrow5}$ was not significant, thus no further significant CMOR decrease occurred. The CMOR changes $\Delta TS_{0\rightarrow1}$ and $\Delta TS_{1\rightarrow5}$ of the samples R20-TNAS were not significant in either case although the analysis of the overall CMOR change $\Delta TS_{0\rightarrow5}$ indicated that a significant strength loss occurred. For the samples R20-SiTNAS, both CMOR changes due to thermal shock were not significant, and neither was the overall CMOR change $\Delta TS_{0\rightarrow5}$. Especially this observation was remarkable, because the repeated thermal shock did not significantly affect the CMOR of the material R20-SiTNAS.

(2) General evaluation of the physical properties and the binder carbon yield

Table 7 summarizes the observed data for the physical properties total porosity, open porosity and true density. Additionally, the binder carbon yield was determined for the coked samples. To evaluate these properties with regard to the factors 'additive combination' (AC) and 'number of thermal shock cycles' (TS), ANOVAs were performed (Table 8). Furthermore, correlation coefficients between the properties of Table 7 were determined to investigate if significant linear relationships existed between these properties.

The ANOVAs in Table 8 showed that the physical properties were all significantly influenced by the factors AC and TS. Regarding the interaction AC:TS, it was significant for the true density and the total porosity. The ANOVA of the binder carbon yield, which was only determined for the coked samples, indicated that the factor AC had no significant influence on this property.

The calculation of correlation coefficients between the investigated properties yielded a value of -0.847 for the open porosity OP and the CMOR. It was significant on a level of 0.01, hence the correlation coefficient exhibited a high significance. This indicated a strongly linear relationship between the open porosity and the CMOR [28].

Table 7: Observed data for total porosity (P), open porosity (OP), true density (TD) and binder carbon yield (BCY).

Property	R20	R20-Si	R20-TNAS	R20-SiTNAS
OP_{0TS} [%]	20.08±1.06	19.06±1.00	19.00 ±0.83	17.89± 0.34
P_{0TS} [%]	22.86 ±1.01	22.60 ±0.71	23.36 ±1.32	21.82 ±0.43
TD_{0TS} [g/cm^3]	3.24 ±0.00	3.26 ±0.00	3.28 ±0.00	3.27 ±0.00
OP_{1TS} [%]	20.62±0.93	20.29 ±0.19	20.21 ±1.27	18.57 ±0.22
P_{1TS} [%]	24.01 ±0.35	24.54 ±1.03	23.85 ±1.26	22.00 ±0.22
TD_{1TS} [g/cm^3]	3.27 ±0.00	3.28 ±0.00	3.28 ±0.00	3.26 ±0.00
OP_{5TS} [%]	20.64±0.69	20.24 ±0.41	19.27 ±0.25	18.78 ±0.11
P_{5TS} [%]	23.46 ±0.59	22.16 ±0.43	22.80 ±0.52	23.13 ±0.55
TD_{5TS} [g/cm^3]	3.25 ±0.00	3.22 ±0.00	3.28 ±0.00	3.29 ±0.00
BCY [%]	60.06 ±12.70	68.83 ±6.71	52.26 ±36.71	74.59 ±42.71

Table 8: *p*-values of the analysis of variance for the total porosity (P), open porosity (OP), true density (TD) and binder carbon yield (BCY) (significant effects on a level ≤ 0.05 marked in italic and on a level ≤ 0.001 bold).

Factor[a]	*p*-value			
	TD	P	OP	BCY
AC	**$<2\cdot10^{-16}$**	*0.0233*	**$3.6\cdot10^{-5}$**	0.796
TS	**$3.2\cdot10^{-13}$**	*0.0188*	*0.0112*	
AC:TS	**$<2\cdot10^{-16}$**	*0.0301*	0.7815	

[a] AC – Additive Combination, TS – Number of thermal shock cycles, AC:TS - Interactions

Furthermore, a moderate correlation was determined for the properties open porosity and total porosity. The correlation coefficient was + 0.660. However, it was statistically significant only on a level of 0.1.

The strong correlation between CMOR and open porosity and the poor correlation between open porosity and total porosity might be caused by the effect of the additives on the materials. The factor 'additive combination' (AC) seemed to influence the open porosity more strongly than the total porosity as is reflected by the much lower *p*-value of the ANOVA for the open porosity ($3.6\cdot10^{-5}$) than for the total porosity (0.0233) (Table 8).

The elevated number of significant influences indicated that complex relationships between reactions due to the additives and the behavior due to thermal shock load had to occur in the material. The correlation coefficients between the observed properties provided compelling evidence that a strong linear relationship between the open porosity and the CMOR existed.

(3) Samples in the coked state

In this section, the properties of the samples after coking are discussed to enable an understanding of the differences between the materials with regard to the initial cold modulus of rupture $CMOR_{0TS}$. The determined correlation coefficients in Section III (2) showed that the open porosity played an important role in the CMOR evolution of all samples in this series. This corresponds to the commonly known relation between pores in a material and its strength. The pores act as failures and their increasing number decreases the strength. The ANOVA yielded a highly significant effect of the factor 'additive combination' on the open porosity with regard to all samples. A Tukey test was performed to identify possible significant differences between the four sample groups after coking. This analysis indicated that only the open porosity of R20-SiTNAS was significantly different (significantly lower) compared to the reference R20. Therefore, the open porosity of the samples in the coked state was only of limited value for understanding the differences in the $CMOR_{0TS}$ of the samples. The total porosity showed no significant differences between the samples in the coked state, either.

The true density exhibited a significant dependence on the additive combination, too, according to the ANOVA in Section III (2). The mean values of the true density in Table 7 are additionally presented in Fig. 2. It illustrates that the true density in the coked state increased in the partial series R20 → R20-Si → R20-TNAS. The true densities of this partial series are all significantly different. An increase of the true density accompanies the formation of phases with a higher true density or increasing quantities of such phases. Table 9 summarizes possible reactions in carbon-bonded alumina caused by thermal load and the presence of oxygen according to the explanations in the introductory section (Section I). It shows firstly that an increasing true density would be related to the formation of SiC whiskers due to the higher true density of SiC (3.21 g·cm^{-3} [12]) compared to Si (2.33 g·cm^{-3} [29]) or C (amorphous C: 1.6 g·cm^{-3} [12]; graphite: 2.22 g·cm^{-3} [29]). Owing to the presence of metallic Si in all samples R20, R20-Si and R20-TNAS and the addition of semi-conductive Si in the samples R20-Si, the formation of SiC whiskers is possible.

The formation of SiC results from the reaction of gaseous species in the material system. Si reacts to SiO(g) owing to the presence of oxygen [30]. Furthermore, CO and CO_2 is provided as a result of oxidation processes of carbon components in the material. The reaction of gaseous SiO and CO results in the growth of whiskers. Wu *et al.* [31] proposed that the presence of graphite in the batch favors especially the formation of whiskers because graphite has

active sites on its surface at elevated temperatures which provide the starting point for the growth of whiskers. Fan *et al.* [32] investigated the formation of whiskers in carbon-bonded alumina also using phenolic resin as binder and graphite as primary carbon. They attributed the formation of their observed whiskers to the reaction mechanism described above. Because of the similarity of the material system in the present study, this mechanism was strongly considered as relevant for the possible formation of SiC whiskers.

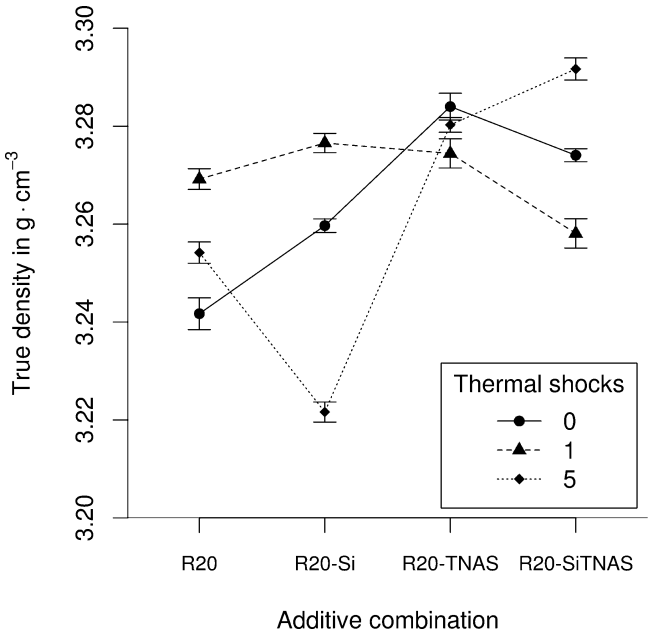

Fig. 2 : Mean values of the true density of the samples after coking (0TS), the first thermal shock cycle (1TS) and the fifth thermal shock cycle (5TS).

The microstructure of the investigated samples in the coked state was presented as SEM images in a previous study [25] by Mertke *et al.* and is summarized as follows: For R20, only single, rarely distributed whiskers were identified. The samples R20-Si showed accumulations of short whiskers. This was in contrast to the previous study by Stein *et al.*[24] who investigated the same sample composition. However, a higher hardening temperature (200 °C in comparison to 180 °C in this study) and a different heating process during coking were used. As this was the only difference in the material processing, it was considered to have an influence on the microstructure. The samples R20-TNAS exhibited rug-like areas with an intensive formation of whiskers, which were longer than for R20-Si. These observations corresponded partly to previous results [4]. Roungos *et al.* [4] presented the formation of Al-O-rich platelets in samples with TN&AS as nanoscaled additives. The formation of these platelets was attributed to the addition of nanoscaled raw materials. It was assumed that these platelets had an increasing effect on the CMOR, similar to whiskers in the microstructure. The differences in the microstructures between the study of Roungos *et al.* [4] and this study were attributed to differences in the mixing procedure of the samples, which might have an influence on the reactions responsible for the whisker formation. In the previous study by Mertke *et al.* [25], which concentrated partly on the same sample series as the present study, the whiskers were examined by means of electron backscattering diffraction. These analyses confirmed that the whiskers consisted of β-SiC phases. This corresponded well to the evolution of the true density in the samples R20, R20-Si and R20-TNAS, shown in Fig. 2. According to the literature [12, 32], the interlocking of the whiskers with each other, with the binding matrix and the granular material was considered to have an increasing effect on the CMOR, which explained the increased $CMOR_{0TS}$ of the samples R20-Si and R20-TNAS in comparison with the reference R20.

Table 9: Possible reactions in the carbon matrix of Si-containing carbon-bonded refractories at elevated temperatures and/or under presence of oxygen, partly according to Yamaguchi[11] (P – porosity, TD – true density, OP – open porosity).

	Reaction/Mechanism	ΔV [%]	Effect on P	TD	OP
1	Oxidation of Si				
1a	$Si(s) + O_2(g) \rightarrow SiO_2(s)$	+115	↓	±0	↓
1b	$Si(s) + 2CO(g) \rightarrow SiO_2(s) + 2C(s)$				
	$C(s) = C_{graphitized}$	+205	↓	↓	↓
	$C(s) = C_{amorphous}$	+240	↓	↓	↓
2	Oxidation of SiC				
2a	$2SiC(s) + 3O_2(g) \rightarrow 2SiO_2(s) + 2CO(g)$	+108	↓	↓	↓
2b	$SiC(s) + 2CO(g) \rightarrow SiO_2(s) + 3C(s)$				
	$C(s) = C_{graphitized}$	+238	↓	↓	↓
	$C(s) = C_{amorphous}$	+288	↓	↓	↓
3	Crystallization of glassy carbon	Max. -28	↑	↑	↑
4	SiC-formation				
	$Si + C \rightarrow SiC$				
	$C(s) = C_{graphitized}$	-28	↑	↑	↑
	$C(s) = C_{amorphous}$	-36	↑	↑	↑
5	Oxidation of C				
	$C(s) + O(g) \rightarrow CO(g)$	-100	↑	↑	↑

The differences in the whisker formation were attributed to the used additives. The nanoscaled additives TN&AS had a very high specific surface (Table 1). This is probably accompanied by a higher reactivity during the coking process and shifted the whisker formation to lower temperatures compared to the reference R20. In the case of R20-Si it was assumed that the semi-conductive silicon – containing additional free electrons due to the doping – influenced the coking reactions, which resulted in the differ-

ences in the microstructure in comparison with the reference R20 [24].

In contrast to the evolution of the true density in the partial series R20 – R20-Si – R20-TNAS, the samples R20-SiTNAS exhibited a decrease in the true density (Fig. 2) although the $CMOR_{0TS}$ increased. This was partly explained by the lower open porosity compared to the reference (see above). However, the SEM images in the previous study [25] indicated that these samples were marked by intensive whisker formation, too. The analysis of the true density demonstrated that it was lower for the samples R20-SiTNAS than for the other samples in the series. The Tukey test yielded that this decrease in the true density was significant. An increased binder yield during the coking process would be a possible mechanism to explain a lower true density in the material (Table 9) because the low density of carbon (amorphous C: 1.6 $g \cdot cm^{-3}$ [12]; graphite: 2.22 $g \cdot cm^{-3}$ [29]) in comparison to the alumina grains would decrease the overall density of the material. Stein *et al.* [22] following Yamaguchi [12] proposed such an effect in carbon-bonded refractories using semi-conductive species. When they are added to a phenolic-resin-containing system, they should yield stabilized carbon structures during the coking process because of their additional free electrons owing to doping or semi-conductive properties at elevated temperatures. This effect could have occurred in the present study, too. The significant decrease in the open porosity of the samples R20-SiTNAS would support this proposed effect because a higher binder carbon yield is linked to a lower open porosity (Table 9).

However, the analysis of the carbon binder yield in this study did not yield significant results as described in Section III (2). No significant effects of the nanoscaled or semi-conductive additives on the binder carbon yield were observed. The experimental data showed a very high variance (Table 7). This might indicate insufficient accuracy or precision of the determination of the carbon content in the samples. These analyses were performed at 950 °C. According to literature data, first decompositions of SiC could take place at this temperature, which would also influence the results of the binder carbon yield analysis [33].

In summary, two points should be highlighted in this section to explain the differences in the cold modulus of rupture after coking. Changes in the open porosity only had a relevant effect on the CMOR for the samples R20-SiTNAS. Regarding the microstructure, the increasing whisker formation due to the single additives TN&AS or semi-conductive silicon and their interlocking were considered very relevant for the mechanical behavior [12, 32]. In the samples R20-SiTNAS the effect of an increased binder carbon yield was proposed according to Stein *et al.* [24] to explain the improved CMOR, although a measurement of the effect had not been possible by that time.

(4) Evolution of the samples under thermal shock load

The ANOVAs in Table 8 show that the thermal-shock-related effects on the total porosity were significant (main effect of TS and interaction AC:TS). The data of the total porosity and its analysis with the Tukey test indicated that the total porosity did not change within the sample groups R20, R20-TNAS and R20-SiTNAS. Only the change of the total porosity in the group R20-Si between the first and the fifth thermal shock cycle was significant. This significant difference, which only occurred to a limited extent, is reflected in the relatively high p-values close to 0.05 for the main effect of TS and the interaction AC:TS on the total porosity. Furthermore, no strong correlations between the total porosity and the CMOR or other physical properties were determined. Therefore, the evolution of the total porosity was not suitable to understand the CMOR evolution.

In analogy to the total porosity, the number of thermal shock cycles had a significant effect on the open porosity on a level of 0.05. The data showed for all samples that the application of thermal shock increased the open porosity compared to the initial state. The Tukey test yielded that for all samples only the first thermal shock cycle caused a significant increase in the open porosity. An increase in the open porosity in combination with the total porosity remaining constant as described above can be explained by the formation of cracks in the material caused by thermal stress during thermal shock [34]. The evolution of the open porosity within the sample groups was comparable because the interaction AC:TS was not significant. Both main effects influenced the open porosity independently according to the available data. It might be possible that the number of investigated samples was insufficient to measure significant differences in the evolution of the open porosity of the samples within each group. This will be investigated in further studies. Therefore, the strong correlation between the open porosity and the CMOR, described in Section III (2), was mainly caused by the global CMOR level within the sample groups and not by a possible evolution of the open porosity of the samples within each group. This is reflected by the large difference in the order of magnitude of the p-values for the main effects TS and AC. The influence of the factor 'additive combination' was highly significant as illustrated by the p-value of $3.6 \cdot 10^{-5}$, whereas the p-value of the factor 'number of thermal shock cycles' was only $1.12 \cdot 10^{-2}$ (Table 8). Hence, for the available data neither the open porosity nor the total porosity alone indicated a sufficient property evolution to understand the CMOR changes of the investigated samples due to thermal shock.

In comparison to the open and total porosity, the ANOVA for the true densities yielded highly significant effects for the TS-related factors. To discuss possible evolutions of this property, Table 9 summarizes reactions occurring in carbon-bonded refractories with Si-species as antioxidants (partly after Yamaguchi [12]). In this study, the thermal shock test was performed with compressed air, which meant that oxygen came into contact with the carbon-bonded material. Owing to the high open porosity, it was very likely that oxygen entered the samples. Therefore, reactions involving oxygen were taken into account. Reactions 1b and 2b correspond to the renewed reaction of CO(g), which formed due to oxidation processes, with other species to form solid carbon deposits. This effect is proposed by Yamaguchi [12]. Table 9 presents the expected effects of these reactions on the true density of the mate-

rial under the assumption that no further coking effects and, related to this, no further shrinkage of the samples occur. As the thermal shock was performed at 950 °C, it was below the initial coking temperature. Therefore, the assumption was probably fulfilled.

In addition to the ANOVA of the true density, the results of the Tukey tests were analyzed. All true densities were significantly different, which corresponded to the low *p*-values in the ANOVA. Furthermore, the results permitted a division of the four sample groups into two types of true density evolution. For the samples R20 and R20-Si the true density increased during the first thermal shock, which was followed by a decrease during the subsequent thermal shocks. According to Table 9, an increase in the true density is caused by the oxidation of C (Reaction 5). A crystallization of glassy carbon would be another possible reaction (Reaction 3). This could be caused by the thermal driving force of the preheating during the thermal shock tests. For the R20-Si-samples the crystallization of glassy carbon to more ordered structures might be enhanced by semi-conductive Si as proposed by Stein *et al.* [24].SiC formation (Reaction 4) could be possible, too, as both sample types contain Si (R20 – metallic Si, R20-Si – metallic and semi-conductive Si). According to Yamaguchi [12], SiC formation can be expected above 600 °C. Especially the formation of SiC whiskers would explain the low CMOR loss during the following thermal shock cycles because interlocking whiskers increase the cold modulus of rupture [12].

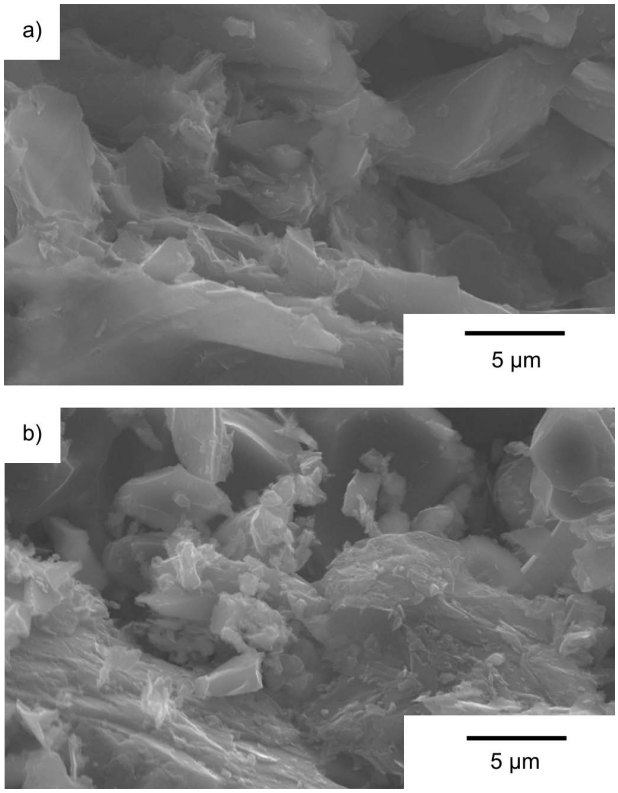

Fig. 3: SEM analysis of R20, (a) after the first thermal shock cycle, (b) after the fifth thermal shock cycle.

Figs. 3a and 4a present the microstructure of R20 and R20-Si after the first thermal shock. In both cases no SiC whiskers were observed. Therefore, it was concluded that the SiC formation was not the dominant process for the increase in the true density. The oxidation of carbon (Reaction 5) or the crystallization of glassy carbon (Reaction 3) were considered to be the dominant processes to explain the measured increase in the true density of R20 and R20-Si.

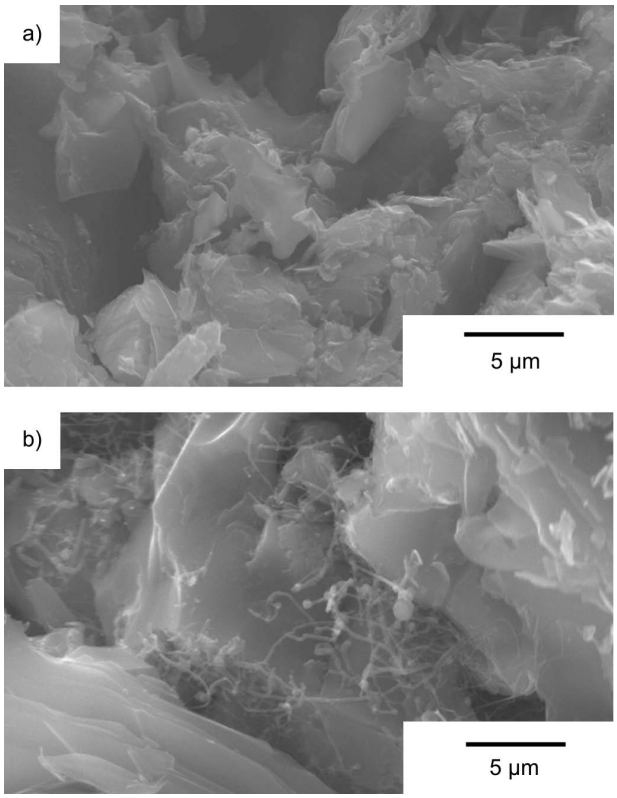

Fig. 4: SEM analysis of R20-Si, (a) after the first thermal shock cycle, (b) after the fifth thermal shock cycle.

Fig. 2 illustrates that both R20 and R20-Si exhibited a decrease in the true density with increasing number of thermal shocks. Figs. 3b and 4b show the microstructure of R20 and R20-Si after the fifth thermal shock. The micrograph of R20-Si exhibited considerable whisker formation. This effect probably caused the lower CMOR loss $\Delta TS_{1\rightarrow5}$ in comparison with the CMOR loss after the first thermal shock (Fig. 1). Furthermore, the observation of these whiskers after the fifth thermal shock cycle indicated that during the alternate heating and quenching of the thermal shock cycles, microstructural changes due to the formation of new phases seem possible. Although the observed whiskers matched very well with the CMOR evolution, they did not correspond to the true density decrease measured after the fifth thermal shock because the formation of SiC is linked to an increase in the true density (Reaction 4). Therefore, other processes had to be taken into account.

The decrease in the true density of R20-Si with increasing number of thermal shock cycles might be related to oxidation processes because of the oxygen contact during these testing cycles. Oxidation processes of Si and SiC (Reactions 1 and 2) cause a decrease in the true density and were likely to occur simultaneously with the SiC formation (Reaction 4) owing to the presence of oxygen. It was considered that these processes overcompensated the increase in the true density by the formation of SiC whiskers

(Reaction 4) or the possible oxidation of carbon (Reaction 5).

For R20, the microstructure remained unchanged in comparison to the coked state and the situation after the first thermal shock (Fig. 3b). SiC whiskers were not observed. Therefore, the oxidation of Si (Reaction 1) was considered to be the dominant reaction for the observed decrease in the true density and to overcompensate a possible oxidation of C (Reaction 5).

The formation of SiO_2 as consequence of the possible oxidation reactions according to Reactions 1 (for R20 and R20-Si) and 2 (for R20-Si) was related to a volume expansion that reduced the porosity of the material. The effect would also correspond well to the CMOR evolution of these samples. The CMOR change $\Delta TS_{1\rightarrow5}$ was not significant, which might be caused by the reduced porosity due to the SiO_2 deposition with increasing number of thermal shock cycles.

The samples R20-TNAS und R20-SiTNAS showed an inverse behavior. This meant that reactions resulting in phases of lower true density dominated the evolution during the first thermal shock. The decrease in the true density after the first thermal shock would be related to the formation of less dense phases. A renewed oxidation of SiC might occur (Reaction 2), which would be linked to the deposition of carbon structures in the case of a reaction path according to Reaction 2b.

To further investigate these possible reactions, SEM analyses were performed for R20-TNAS and R20-SiTNAS after the first and fifth thermal shock.

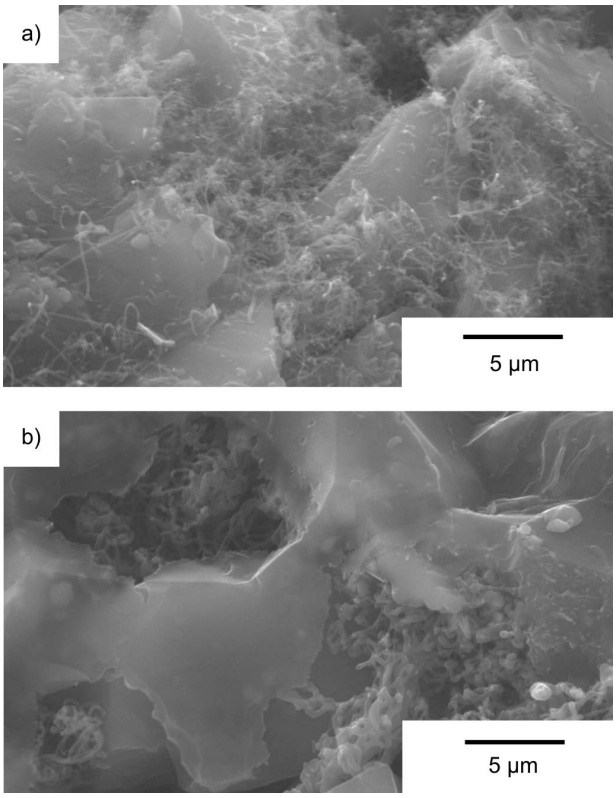

Fig. 5: SEM analysis of R20-TNAS, (a) after the first thermal shock cycle, (b) after the fifth thermal shock cycle.

Fig. 5a illustrates the microstructure of R20-TNAS after the first thermal shock cycle. The short rug-like whisker areas which formed during the coking process developed into shorter whiskers and the number of whiskers seemed to have decreased. This corresponded to the observed true density decrease after the first thermal shock cycle (Fig. 2). In Fig. 5b the structural state after the fifth thermal shock can be seen. Although their number seemed to have remained constant, the whiskers' length and diameter had increased. This would explain the renewed increase in the true density after the fifth thermal shock (Fig. 2).

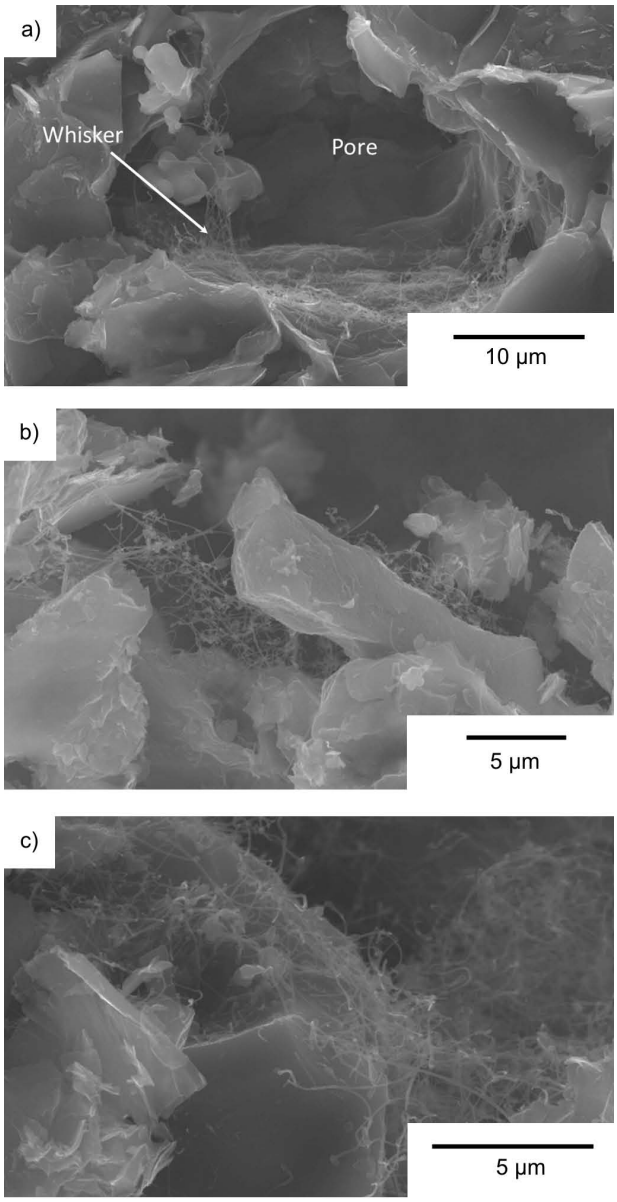

Fig. 6: SEM analysis of R20-SiTNAS after the first thermal shock.

Figs. 6 and 7 show the microstructural evolution of R20-SiTNAS. Fig. 6 shows an increase in the amount of whiskers in the material after the first thermal shock. Especially remarkable was the increasing length of the grown whiskers. The whiskers were especially noticed in the voids of the samples. The SEM images after the fifth thermal shock showed a further increase of the number of whiskers (Fig. 7) although the whiskers were shorter than after the first thermal shock. They resembled the rug-like areas, as in R20-TNAS after coking. The continuous increase in the whisker number during the thermal

shock tests did not correspond to the observed true density decrease after the first thermal shock. This will be investigated in further studies.

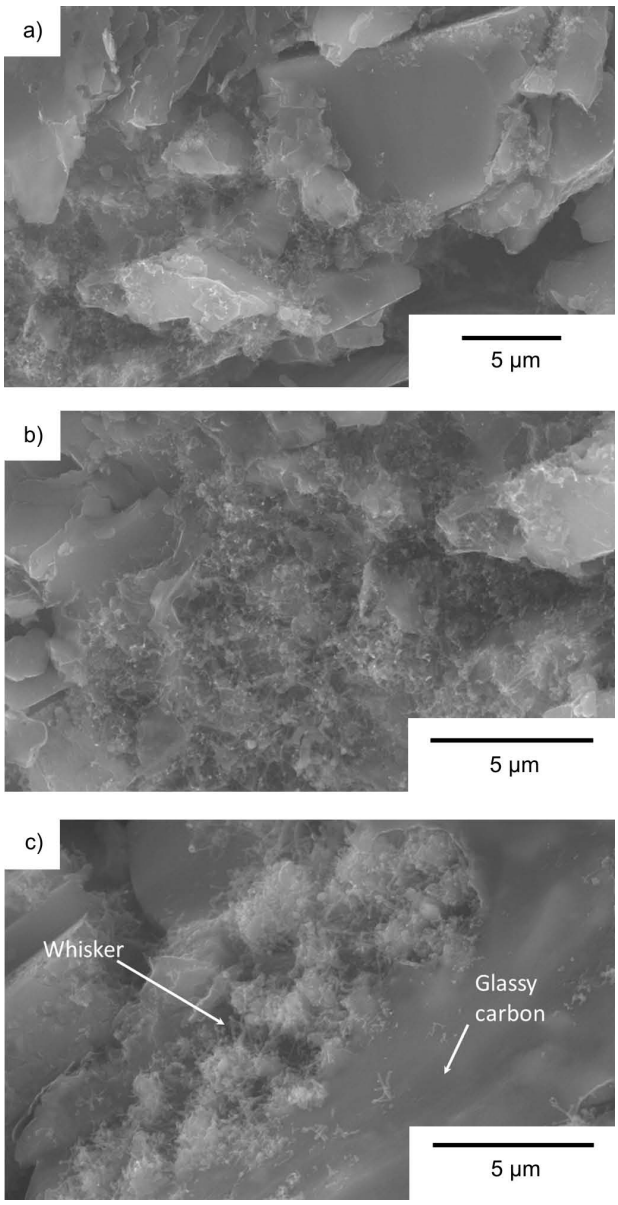

Fig. 7: SEM analysis of R20-SiTNAS after the fifth thermal shock.

The stronger whisker formation of R20-TNAS and R20-SiTNAS in comparison with the samples R20 and R20-Si was probably caused by the presence of the nanoscaled additives TN&AS. Owing to their high specific surface area (Table 1), they provided an additional reactivity, which intensified whisker formation. The earlier formation of the whiskers and their reactions in comparison with R20-Si might have dominated the microstructural evolution during the first thermal shock cycle.

It was remarkable that the samples of R20-TNAS after coking and R20-SiTNAS after the fifth thermal shock exhibited predominantly the rug-like whisker areas. Simultaneously, these samples showed comparatively high CMOR values within their sample group (Fig. 1). In the data of Fan *et al.* [32], it can also be observed that samples with rug-like whisker formations exhibited the highest CMOR values in their study. A possible explanation could be the improved interlocking and bonding between aggregates and the surrounding matrix. For example, a closure of developing gaps during coking caused by differences in the absolute thermal expansions of the carbon matrix and the aggregates [35] seems possible.

Additionally, for R20-SiTNAS, it was observed that a renewed formation of glassy carbon layers occurred (Fig. 7c), which were interlocked with the fiber system of the whiskers. If whisker formation was the dominating process compared to the formation of glassy carbon, the true density would increase. This would also match with the observed data for R20-SiTNAS presented in Fig. 2 where an increase in the true density of the samples R20-SiTNAS after the fifth thermal shock is shown. Therefore, it was proposed that these reactions could provide a self-healing capacity of the material because the renewed formation of glassy carbon would seal failures in the material formed due to thermal shock. It was assumed that the carbon necessary for the formation of these structures originated from the release of CO resulting from oxidation processes during the thermal shocks. The testing procedure comprised the alternate heating of the samples in reducing atmosphere and quenching in compressed air. Because of the open porosity, both the inner and outer surface were in contact with oxygen. It was therefore considered likely that oxygen was present in the samples at the beginning of each heating cycle to participate at possible reactions. It was assumed that the semi-conductive silicon in the batches influenced these reactions because of its ability to provide additional electrons [24]. This effect of the formation of such carbon structures is shown schematically in Fig. 8. Yamaguchi [12] also proposed the formation of carbon deposits, e.g. because CO(g) as product of oxidation reactions reacts further with other species resulting in solid carbon deposits (Reaction 1b and 2b in Table 9). This reaction would also be accompanied by the deposition of SiO_2, which reduces the porosity of the material, which corresponded to the CMOR evolution of the samples.

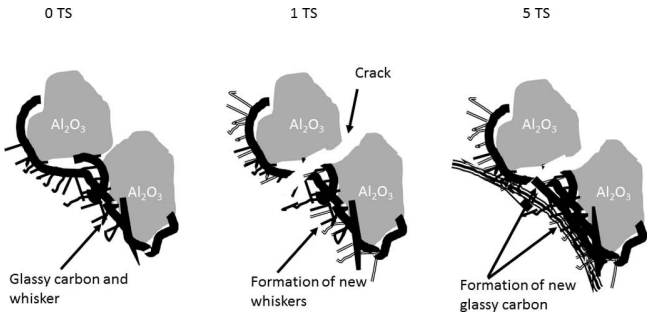

Fig. 8: Schematic model of microstructural evolution during the thermal shock cycles of R20-SiTNAS.

IV. Conclusions

This study investigated the combined effect of nanoscaled additives (carbon nanotubes and nanoscaled alumina) and semi-conductive silicon on carbon-bonded alumina with the reduced content of primary carbon of 20 wt%. It focused especially on the initial cold modulus of rupture and its evolution after thermal shock.

The use of the single additive groups or their combination yielded an increased initial strength compared to the reference without additives. It was shown that the combination of the additives resulted in a material that exhibited no statistically significant decrease in the cold modulus of rupture after thermal shock. To enable understanding of these effects, physical properties of the investigated materials such as total porosity, open porosity and true density were determined. The data indicated very complex reactions in the microstructure. Several reactions occurred simultaneously. The combination of all additives caused a decrease in the open porosity. The available data of the true density analysis corresponded partly to the possible reactions. Especially the formation of SiC whiskers was considered to be important in the initial coking process and during the thermal shock cycles. Furthermore, it was proposed that during the thermal shock cycles, a deposition of carbon due to oxidation processes followed by reactions with the additives, especially the semi-conductive silicon, occurred. This relocated carbon might have a self-healing effect on the refractory matrix.

Future studies will concentrate on observations of the microstructure after the coking process and its evolution with thermal shock. Additionally, a further reduction of the primary carbon content below 20 wt% will be investigated.

Acknowledgment

The authors would like to thank the DFG (German Research Foundation) for funding this work within the Priority Program 1418 under grant number AN 322/16. The authors would also like to thank Dr G. Schmidt for the SEM examinations and Dr S. Schafföner for proof reading.

References

1 Salmang, H., Scholze, H., Telle, R.: Ceramics, in German, 7th Edition, Springer-Verlag, Berlin, Heidelberg, 2007.

2 Pierson, H.O: Handbook of carbon, graphite, diamond and fullerenes – properties, processing and applications, Noyes Publications, Park Ridge, New Jersey, 1993.

3 Krüger, A.: New carbon materials – an introduction, in German, 1st edition. B.G. Teubner Verlag, Wiesbaden, 2007.

4 Roungos, V., Aneziris, C.G.: Improved thermal shock performance of Al_2O_3-C refractories due to nanoscaled additives, Ceram. Int., **38**, [2], 919 – 92, (2012).

5 Gardziella, A.: Chemistry and physics of duroplastic resins in plastics handbook vol. 10 duroplastics, in German, Editors: Becker, G.W., Braun, D., Woebcken, W., Carl HanserVerlag, Munich, Vienna, 1988.

6 Lewis, I.C.: Chemistry of carbonization, carbon, **20** [6], 519 – 529, (1982).

7 Guan, G., Kusakabe, K., Ozono, H., Taneda, M., Uehara, M., Maeda, H.: Preparation of carbon microparticle assemblies from phenolic resin using an inverse opal templating method, J.Mater. Sci., **42**, [24], 10196 – 10202, (2007).

8 Bundes-Immissionsschutzgesetz BImSchG: Mit Durchführungsverordnungen, Emissionshandelsrecht, TA Luft und TA Lärm [Germany's Federal Ambient Pollution Control Act]. 10th edition, Deutscher Taschenbuch Verlag, 2010.

9 Kyoto Protocol, Third International Conference of the Parties Kyoto, Japan, December 11, 1997.

10 Buhr, A.: Trends in clean steel technology and refractory engineering, Plenary Speech, 14th Unified International Technical Conference on Refractories – UNITECR 2015, 15.-18.09.15, Vienna

11 Khezrabadi, M.N., Javadpour, J., Rezaie, H.R., Naghizadeh, R.: The effect of additives on the properties and microstructures of Al_2O_3-C refractories, J. Mater. Sci., **41**, [10], 3027 – 3032, (2006).

12 Yamaguchi, A.: Self-repairing function in the carbon-containing refractory, Int. J. Appl. Ceram. Tec., **4**, [6], 490 – 495, (2007).

13 Sunayama, H., Kawahara, M., Mitsuo, T., Sumitomo, K.: The effect of B_4C addition on the oxidation resistance of Al_2O_3-C and Al_2O_3-SiC-C refractories, Proceedings of the Unified International Technical Conference on Refractories, 1997.

14 Zhang, S., Yamaguchi, A.: A comparison of Al, Si and Al_4SiC_4 added to Al_2O_3-C refractories, Proceedings of the Unified International Technical Conference on Refractories. New Orleans, USA, 1997.

15 Vieira Jr., W., Rand, B.: The nature of the bond in silicon-containing alumina-carbon refractory composites – Part I, Proceedings of the Unified International Technical Conference on Refractories. New Orleans, USA, 1997.

16 Zhang, S.: Next generation carbon-containing refractory composites, Adv. Sci. Tech, **45**, 2246 – 2253, (2006).

17 Luhrsen, E., Ott, A.: Immersion nozzles for metal melts. U.S. Patent 5, 171, 495, 15, 1992.

18 Wang, T., Yamaguchi, A.: Antioxidation behavior and effect of Al8B4C7 added to carbon-containing refractories, J. Ceram. Soc. Jpn., **108**, [9], 818 – 822, (2000).

19 Roungos, V., Aneziris, C.G., Berek, H.: Novel Al_2O_3-C refractories with less residual carbon due to nanoscaled additives for continuous steel casting applications, Adv. Eng. Mater., **14**, [4], 255 – 264, (2012).

20 Yamaguchi, A., Zhang, S., Yu, J.: Effect of refractory oxides on the oxidation of graphite and amorphous carbon, *J. Am. Ceram. Soc.*, **79**, [9], 2509 – 2511, (1996).

21 Aneziris, C.G., Hubálková, J., Barabás, R.: Microstructure evaluation of MgO-C refractories with TiO_2- and Al-additions, *J. Eur. Ceram. Soc.*, **27**, [1], 73 – 78, (2007).

22 Stein, V.: Contribution to the characteristic improvement of carbon bonded doloma refractories by addition of functional ceramic materials, Freiberger Forschungsheft, Reihe A, 905, (2011).

23 Stein, V., Aneziris, C.G., Guéguen, E., Hill, K.: A prospective way to reduce emissions in secondary steel making metallurgy by application of functionalized doloma carbon refractories, Int. J. Appl. Ceram. Tec., **9**, [3], 615 – 624, (2012).

24 Stein, V., Aneziris, C.G.: Low-carbon carbon bonded alumina refractories for functional components in steel technology, *J. Ceram. Sci. Tech.*, **5**, [2],115 – 124, (2014).

25 Mertke, A., Aneziris, C.G.: The influence of nanoparticles and functional metallic additions on the thermal shock resistance of carbon bonded alumina refractories, *Ceram. Int.*, **41**, [1], 1541 – 1552, (2015).

26 Kunz, G.: Ladle refractories for clean steel production, *RHI Bull.*, **2**, 30 – 40, (2010).

27 Fruhstorfer, J., Schafföner, S., Werner, J., Wetzig, T., Schöttler, L., Aneziris, C.G., Thermal schock performance of refractories for application in steel ingot casting, *J. Ceram. Sci. Tech.*, DOI: 10.4416/JCST2016 – 00010, (2016).

28 Montgomery, D.C., Runger, G.C., Hubele, N.F.: Engineering statistics, 4th Edition, Hoboken, NJ: Wiley, 2007.

29 Lautenschläger, K.-H.; Schröter, W., Wanninger, A.: Pocket book of chemistry, in German, 20., revised and extended addition, reprint, Frankfurt am Main, 2007

[30] Tang, C.C., Fan, S.S., Dang, H.Y., Zhao, C., Zhang, P., Li, P., Gu, Q.: Growth of SiC nanorods prepared by carbon nanotubes-confined reaction, *J. Cryst. Growth*, **210**, [4], 595 – 599, (2000).

[31] Wu, Y.J., Wu, J.S., Qin, W., Xu, D., Yang, Z.X., Zhang, Y.F., Synthesis of β-SiC nanowhiskers by high temperature evaporation of solid reactants, *Mater. Lett.*, **58**, [17 – 18], 2295 – 2298, (2004).

[32] Fan, H., Li, Y., Sang, S., Microstructures and mechanical properties of Al_2O_3-C refractories with silicon additive using different carbon sources, *Mat. Sci. Eng. A*, **528**, [7 – 8] 3177 – 3185, (2011).

[33] Tran, H.K., Sawko, P.M.: Thermal degradation study of silicon carbide threads developed for advanced flexible thermal protection systems, NASA Technical Memorandum 103952, 1992

[34] Fruhstorfer, J., Möhmel, S., Thalheim, M., Schmidt, G., Aneziris, C.G.: Microstructure and strength of fused high alumina materials with 2.5 wt% zirconia and 2.5 wt% titania additions for refractory applications, *Ceram. Int.*, **41**, [9], 10644 – 10653, (2015).

[35] Werner, J., Aneziris, C.G., Dudczig, S.: Young's modulus of elasticity of carbon-bonded alumina materials up to 1450°C, *J. Am. Ceram. Soc.*, **96**, [9], 2958 – 2965, (2013).